Geosci. Model Dev. Discuss., 8, 4245–4292, 2015
www.geosci-model-dev-discuss.net/8/4245/2015/
doi:10.5194/gmdd-8-4245-2015

Geoscientific Model Development Discussions
Open Access

Open-source modular solutions for flexural isostasy: gFlex v1.0

A. D. Wickert[1,2]

[1]Institut für Erd- und Umweltwissenschaften, Universität Potsdam, Potsdam-Golm, Germany
[2]Department of Earth Sciences, University of Minnesota, Minneapolis, MN, USA

Received: 6 March 2015 – Accepted: 29 April 2015 – Published: 2 June 2015

Correspondence to: A. D. Wickert (andrew.wickert@uni-potsdam.de)

Published by Copernicus Publications on behalf of the European Geosciences Union.

Abstract

Isostasy is one of the oldest and most widely applied concepts in the geosciences, but the geoscientific community lacks a coherent, easy-to-use tool to simulate flexure of a realistic (i.e. laterally heterogeneous) lithosphere under an arbitrary set of surface loads. Such a model is needed for studies of mountain-building, sedimentary basin formation, glaciation, sea-level change, and other tectonic, geodynamic, and surface processes. Here I present gFlex, an open-source model that can produce analytical and finite difference solutions for lithospheric flexure in one (profile) and two (map view) dimensions. To simulate the flexural isostatic response to an imposed load, it can be used by itself or within GRASS GIS for better integration with field data. gFlex is also a component with the Community Surface Dynamics Modeling System (CSDMS) and Landlab modeling frameworks for coupling with a wide range of Earth-surface-related models, and can be coupled to additional models within Python scripts. As an example of this in-script coupling, I simulate the effects of spatially variable lithospheric thickness on a modeled Iceland ice cap. Finite difference solutions in gFlex can use any of five types of boundary conditions: 0-displacement, 0-slope (i.e. clamped); 0-slope, 0-shear; 0-moment, 0-shear (i.e. broken plate); mirror symmetry; and periodic. Typical calculations with gFlex require $\ll 1$ s to ~ 1 min on a personal laptop computer. These characteristics – multiple ways to run the model, multiple solution methods, multiple boundary conditions, and short compute time – make gFlex an effective tool for flexural isostatic modeling across the geosciences.

1 Introduction

Flexure of the lithosphere is a frequently observed processes by which loads bend the elastic outer shell of Earth or other planets (Watts, 2001; Watters and McGovern, 2006). The sources of these loads are wide-ranging (Fig. 1), encompassing volcanic islands and seamounts (Watts, 1978; Watts and Zhong, 2000), mountain-belt-forming

GMDD
8, 4245–4292, 2015

thrust sheets their associated subsurface loads (Karner and Watts, 1983; Stewart and Watts, 1997), sedimentary basins (Watts et al., 1982; Heller et al., 1988; Dalca et al., 2013), continental ice sheets (Le Meur and Huybrechts, 1996; Gomez et al., 2013), lakes (Passey, 1981; May et al., 1991), seas and oceans (Govers et al., 2009; Luttrell and Sandwell, 2010), extensional tectonics (negative loads) (Wernicke and Axen, 1988), erosion (negative loads) (McMillan et al., 2002), mantle plumes (basal buoyant and therefore negative loads) (D'Acremont et al., 2003), and more.

Analytical theory to describe deflections of the lithosphere under loads has evolved significantly over the past 160 years (Watts, 2001). The development of this theory started with simple approximations of perfect buoyant compensation of loads by a lithosphere with no finite strength overlying a mantle of known density (Airy, 1855; Pratt, 1855). These approximations allowed surveyors to explain the observed lack of significant gravity anomalies around large mountain belts (cf., Göttl and Rummel, 2009). While this theory, called isostasy, revolutionized the way topography was viewed on the Earth, more realistic solutions for isostatic deflections of the surface of Earth take into account the bending, or flexure, of a lithospheric plate of finite strength. By bending over distances of several 10's to 100's of km, the lithosphere low-pass filters a discontinuous surface loading field into a smoothed solid-Earth response.

Even though the early geological theories of Pratt (1855) and Airy (1855) focused on simple buoyancy, the differential equation basis for solving lithospheric bending already existed at that time. Bernoulli (1789) and Germain (1826, and earlier work) developed the first differential-equation-based theories for plate bending. Lagrange (1828) reviewed the prize that Germain won in 1811 for her work on elastic plate flexure, and, on realizing an error in the lumping of terms due to Germain's incorporation of an incorrect formula by Euler (1764), corrected it and produced the first complete flexure equation (see reviews by Todhunter and Pearson, 1886; Ventsel et al., 2002). Around the same time, Cauchy (1828) and Poisson (1828) better connected elasticity theory to plate bending problems. These works predated Kirchhoff (1850), who developed "classical" or "Kirchhoff" plate theory that remains in use today (Ventsel et al., 2002).

While many further advances have been made (e.g., Love, 1888; Timoshenko et al., 1959) especially for structural and aeronautical engineering, it is the classical Kirchhoff plate theory that has been used most widely for geological applications (e.g., van Wees and Cloetingh, 1994). Comer (1983) tested classical Kirchhoff plate theory, which is a "thin-plate" theory that simplifies the plate geometry and therefore the mathematics required to solve for it, against a "thick-plate" theory of lithospheric flexure. While this thick-plate theory relaxes several approximations, its solutions are very similar to those for thin-plate flexure (Comer, 1983).

In the first half of the twentieth century, Vening Meinesz (1931, 1941, 1950) and Gunn (1943) applied analytical solutions of the plate theory of Kirchhoff (1850) to geological problems. They employed analytical solutions that relate the curvature of the bending moment of a plate of uniform elastic properties to an imposed surface point load, line load, or sinusoidal load. These load solutions could be used to compute flexural response to any arbitrary sum of individual loads in either the spatial or spectral domain, due to the linear nature of the biharmonic flexure equation (Eqs. 1 and 2), and may be combined with a variety of boundary conditions (Watts, 2001).

Computational advances allowed discretized models to replace purely analytical solutions. These models fall into one of several categories. Many take advantage of the linear nature of the flexure equation for constant elastic thickness to superimpose analytical solutions of point loads (in the spatial domain) or sinusoidal loads (in the wavenumber domain) in order to produce the flexural response to an arbitrary load (Comer, 1983; Royden and Karner, 1984). Other models produce numerical solutions to the thin plate flexure equation by solving the local derivatives in plate displacement with numerical (mostly finite difference) methods (e.g., Bodine et al., 1981; van Wees and Cloetingh, 1994; Stewart and Watts, 1997; Pelletier, 2004; Govers et al., 2009; Sacek and Ussami, 2009; Wickert, 2012; Braun et al., 2013). This latter category of models allow for variations in the elastic thickness of the plate, a factor of growing importance as variations in elastic thickness through space and time are increasingly recognized, measured, and computed (e.g., Watts and Zhong, 2000; Watts, 2001; Van

GMDD
8, 4245–4292, 2015

der Lee, 2002; Flück, 2003; Pérez-Gussinyé and Watts, 2005; Pérez-Gussinyé et al., 2007, 2009; Tassara et al., 2007; Kirby and Swain, 2009, 2011; Kirby, 2014; Lowry and Pérez-Gussinyé, 2011; Tesauro et al., 2009, 2012b, a, 2013; Braun et al., 2013). In spite of these efforts, the community currently lacks a robust, easy-to-use, generalized tool for flexural isostatic solutions that can be used by modelers and data-driven scientists alike.

Here I introduce a broadly implementable open-source package of solutions to flexural isostasy. This package, called gFlex (for GNU flexure), advances and makes greatly more accessible an earlier model, generically called "flexure" (Wickert, 2012). gFlex has been released under the GNU General Public License (GPL) version 3 and is made available to the public at the University of Minnesota Earth-surface GitHub organizational repository, at https://github.com/umn-earth-surface/gFlex, and through the Python Package Index (PyPI). This allows for rapid collaborative editing of the source code and easy automated installation. It is written in Python (e.g., van Rossum and Fred L. Drake, 2012) for easy interoperability with a range of other programming languages, models, and geographic information systems (GIS) packages, and to take advantage of the numerical packages for Python that allow much more rapid matrix solutions than would be typical with a more basic interpreted language (Jones et al., 2001; Davis, 2004; Oliphant, 2007; van der Walt et al., 2011). See Sect. 5 for further information on obtaining and running gFlex.

gFlex can solve plate flexure in two major ways (Fig. 2). First, it can produce analytical solutions to flexural isostasy generated by superposition of local solutions to point loads in the spatial domain (i.e. as a sum of Green's functions) (e.g., Royden and Karner, 1984). These use biharmonic equation for plate flexure with uniform elastic properties (Eqs. 1 and 2) (Bodine et al., 1981). Second, it can compute finite difference solutions for both constant and arbitrarily varying lithospheric elastic thickness structures. These solutions follow the work of van Wees and Cloetingh (1994), and hence Braun et al. (2013), except that gFlex does not incorporate terms for end loads but does include a wider range of implementable boundary conditions (Table 1). gFlex can be run as a standalone program with an input file, as a component of the in-development Landlab landscape modeling framework (Hobley et al., 2013; Tucker et al., 2013) and by extension as a component within the Community Surface Dynamics Modeling System (CSDMS) (Syvitski et al., 2011; Overeem et al., 2013), or as a pair of “add-ons” to GRASS GIS (Neteler et al., 2012). The GRASS GIS implementation is particularly important, as it provides pre-built and standardized command-line and graphical interfaces and the ability to directly pull inputs from and compare solutions against field data in their native coordinate systems.

2 Methods and model development

Two solution types for flexural isostasy are provided in gFlex, and these are formulated for both one-dimensional (line load, assumed to extend infinitely in an orientation orthogonal to the line along which the equation is solved) and two-dimensional (point load) cases. The derivation that forms the basis for both of these is provided in Appendix A, and similar approaches to this derivation may be found in the work of Timoshenko et al. (1959) and Turcotte and Schubert (2002). The analytical and finite difference approaches are compared and shown to approximate each other well in Fig. 3.

2.1 Superposition of analytical solutions

The first solution type takes advantage of the linear nature of the analytical solution for flexure of a plate of constant thickness and elastic properties when subjected to a point or line load. These solutions may be superposed (i.e. summed) in space to compute the full flexural response. The second approach is to solve the equation for lithospheric flexure as a matrix equation by employing a finite difference scheme. This employs a sparse matrix elimination solver (e.g., Davis, 2004). The primary gFlex finite difference solution follows the approach of van Wees and Cloetingh (1994) to permit computations with steep gradients in flexural rigidity (Appendix A2), but it also offers the discretization of Govers et al. (2009).

The analytical solution imposes the assumption that scalar flexural rigidity, D, is uniform. This leads to biharmonic expressions for plate bending in one and two dimensions, respectively:

$$D\frac{\mathrm{d}^4 w}{\mathrm{d}x^4} + \Delta\rho g w = q \tag{1}$$

$$D\nabla^4 w = D\frac{\mathrm{d}^4 w}{\mathrm{d}x^4} + D\frac{\mathrm{d}^4 w}{\mathrm{d}y^4} + 2D\frac{\mathrm{d}^4 w}{\mathrm{d}x^2\mathrm{d}y^2} + \Delta\rho g w = q \tag{2}$$

These equations are linearizable, and therefore can be solved by superposition of analytical solutions. In gFlex, this is done in the spatial domain on both structured grids and as a response to an arbitrarily placed set of point loads. Spectral solutions are possible (Stephenson, 1984; Stephenson and Lambeck, 1985) and efficient using fast Fourier transform algorithms (cf. Welch, 1967), but have not been implemented. The 1- and two-dimensional solutions for lithospheric flexure take the form of an exponentially damped sinusoid. In one dimension, this is represented by the following expression:

$$w_i = q\frac{\alpha_{1\text{-D}}^3}{8D}e^{\frac{(x-x_i)}{\alpha_{1\text{-D}}}}\left[\cos\left(\frac{x-x_i}{\alpha_{1\text{-D}}}\right) + \sin\left(\frac{x-x_i}{\alpha_{1\text{-D}}}\right)\right] \tag{3}$$

Here, the i subscript indicates that this is the response to a line-load at a single x position, x_i. $\alpha_{1\text{-D}}$ is the one-dimensional flexural parameter, defined by Vening Meinesz (1931) (following Hertz, 1884):

$$\alpha_{1\text{-D}} = \left[\frac{4D}{(\Delta\rho)g}\right]^{1/4} \tag{4}$$

The significance of the flexural parameter is that the flexural wavelength, λ_α is related to the flexural parameter as $\lambda_\alpha = 2\pi\alpha$. The distance from a point load to the first flexural bulge ("forebulge") that it creates around its local depression, for example, is a flexural half-wavelength, $\pi\alpha$. This nature of plate bending as an exponentially decaying periodic function can be seen most easily in the one-dimensional analytical (constant T_e) solution in Eq. (3).

Brotchie and Silvester (1969) derived that the exponentially damped sinusoid due to a point load in two dimensions should be expressed by a modified Kelvin–Bessel function (Abramowitz and Stegun, 1972), and this solution has been broadly applied (e.g., Lambeck, 1981; McNutt and Menard, 1982).

$$w_{i,j} = q\frac{\alpha_{2\text{-D}}^2}{2\pi D}\mathrm{kei}\left(\frac{\sqrt{(x-x_i)^2+(y-y_j)^2}}{\alpha_{2\text{-D}}}\right) \quad (5)$$

$$\alpha_{2\text{-D}} = \left[\frac{D}{(\Delta\rho)g}\right]^{1/4} \quad (6)$$

The subscripts i,j indicate that this is the flexural response to a single point load at the x and y positions x_i and y_j. The two-dimensional flexural parameter, $\alpha_{2\text{-D}}$, contains D instead of $4D$ in the numerator because it does not need to include implicit loads and deflections along the y orientation that are required in the 1-D line load plate bending case.

Lithospheric flexure calculated by superposition of analytical solutions can be represented as a simple sum across all line loads q_l or point loads q_p:

$$w = \sum_{q_\mathrm{l}} w_i \quad (1D) \quad (7)$$

$$w = \sum_{q_\mathrm{p}} w_{i,j} \quad (2D) \quad (8)$$

For a given elastic thickness, each flexural response to a line or point load is similar in shape, but different in amplitude. Therefore, for rectilinear grids in 2 dimensions

GMDD
8, 4245–4292, 2015

with dx and dy that are uniform but not necessarily equal, solution time is optimized by generating a template deflection array that has twice the linear dimensions of the solution array, centering this template over the load, scaling its magnitude to the computed flexural response, and summing the scaled templates produced for each cell. One-dimensional solutions are rapid enough that this optimization technique has not been found to be necessary. Within gFlex, this solution type is termed "SAS", which stands for "Superposition of Analytical Solutions".

The analytical solution response to point or line loads can also be computed for a scattered set of loads and a scattered (and not necessarily the same) set of points at which the flexural response is calculated. This solution type is termed "SAS_NG", which stands for, "superposition of Analytical Solutions: No Grid". Because it lacks the grid uniformity that permits the a solution template to be used, its computational time is not optimized in this way (Sect. 2.4).

2.2 Finite difference solutions

Finite difference solutions in one and two dimensions employ Eqs. (A20) and (A21), respectively. For these solutions, dx and dy may differ from one another, but must be constant in space. First, for the one-dimensional solution, the expansion of Eq. (A20) is:

$$D\frac{\partial^4 w}{\partial x^4} + 2\frac{\partial D}{\partial x}\frac{\partial^3 w}{\partial x^3} + \frac{\partial^2 D}{\partial x^2}\frac{\partial^2 w}{\partial x^2} + \Delta\rho g w = q \tag{9}$$

The two-dimensional solution is based on an expansion of Eq. (A21) (van Wees and Cloetingh, 1994):

$$D\frac{\partial^4 w}{\partial x^4} + D\frac{\partial^4 w}{\partial y^4} + 2D\frac{\partial^4 w}{\partial x^2 \partial y^2}$$
$$+ 2\frac{\partial D}{\partial x}\frac{\partial^3 w}{\partial x^3} + \frac{\partial^2 D}{\partial x^2}\frac{\partial^2 w}{\partial x^2} + 2\frac{\partial D}{\partial y}\frac{\partial^3 w}{\partial y^3} + \frac{\partial^2 D}{\partial y^2}\frac{\partial^2 w}{\partial y^2}$$

GMDD
8, 4245–4292, 2015
Flexure of the Lithosphere: gFlex v1.0
A. D. Wickert

$$+\nu\frac{\partial^2 D}{\partial y^2}\frac{\partial^2 w}{\partial x^2}+\nu\frac{\partial^2 D}{\partial x^2}\frac{\partial^2 w}{\partial y^2}+2\frac{\partial D}{\partial x}\frac{\partial^3 w}{\partial x\partial y^2}+2\frac{\partial D}{\partial y}\frac{\partial^3 w}{\partial x^2\partial y}$$
$$+2(1-\nu)\frac{\partial^2 D}{\partial x\partial y}\frac{\partial^2 w}{\partial x\partial y}+\Delta\rho g w=q \tag{10}$$

These equations are discretized using a second-order-accurate centered finite difference approximation (Fornberg, 1988, Table 1).

Finite difference solutions in two dimensions may also be generated following the solution and discretization of Govers et al. (2009), which produces solutions for a more limited range of flexural rigidity variations.

The finite difference solution is computed as a linear matrix equation,

$$\mathbf{A}\boldsymbol{W}=\boldsymbol{Q}, \tag{11}$$

where **A** is a sparse matrix of operators from a linear decomposition of Eq. (A20) or (A21), $\boldsymbol{W}$ is a vector of deflections (typically unknown), and $\boldsymbol{Q}$ is a vector of imposed loads (typically known). It is solved directly by using the sparse LU factorization package UMFPACK (Davis, 2004) or, at the user's choice, iteratively with one of the many solvers that are available with the SciPy (Scientific Python) package (Jones et al., 2001).

2.3 Boundary conditions

gFlex supports a number of boundary conditions, and these are summarized in Table 1 and schematically drawn in Fig. 4. The finite difference (sparse matrix) numerical solutions can freely define any combination of no-displacement-and-no-slope (0Displacement0Slope), no-bending-moment-and-no-shear (0Moment0Shear), no-slope-and-no-shear (0Slope0Shear), and Mirror boundaries. Periodic boundaries may be mixed with any combination of the aforementioned boundary conditions, with the requirement that they exist on both sides of the deflection array, as having (for example) deflections at the west end of the array sensitive to loading and deflections to the east but the east not be sensitive to the west is nonsensical. Superposition of analytical solutions naturally produce a 0-displacement boundary at infinite distance from each point load (NoOutsideLoads). This can be seen by computing the solutions of Eqs. (3) and (5) as $x \to \infty$ and $y \to \infty$. Each of these boundary conditions can be related to geological processes or locations that one may wish to model (Fig. 5).

The "0Displacement0Slope" (or "clamped") boundary condition (Fig. 4a) may be used to approximate a "NoOutsideLoads" case for the finite difference solutions (Fig. 3). When placed one flexural wavelength away from a point or line load, the surface displacement should for a plate of constant elastic thickness be $\sim 0.2\,\%$ of that at the point of maximum deflection, which is negligible compared to most sources of geological error. It is conceivable that a difference in elastic thickness in a continuous plate may exist that is so great that the thicker plate can be approximated to not bend; a 0Displacement0Slope boundary condition may also be used to simulate this, though one must debate whether to do this or to compute the flexural response across a plate with prescribed elastic thickness variability.

The "0Moment0Shear" boundary condition (Fig. 4b) means that the edge of the plate is completely free to flex, like the cantilevered end of diving board. This is appropriate for places in which the elastic thickness of the lithosphere goes to zero. Such "broken plate" boundary conditions have been used in analytical solutions to simulate flexure of the lithosphere beneath the Hawaiian Volcanoes, where heating significantly weakens the lithosphere, although the (albeit moving) point source of heat means that this may be only an approximation for a boundary condition along a whole edge of a model (Wessel, 1993); zones beneath mountain ranges where sufficient deformation may weaken the lithosphere (Stewart and Watts, 1997), although the approximation of a broken plate may with more data be replaced by a more realistic elastic thickness structure as these can be generated with methods of increasing sophistication (Tesauro et al., 2013; Kirby, 2014); and as a solution for continental rift zones (Burov et al., 1994), which might most closely approximate a linear discontinuity in an oth-

GMDD
8, 4245–4292, 2015

erwise thick lithosphere. While this is also a possible boundary condition in the analytical case, the difficulty in finding a place where the lithosphere suddenly breaks without a gradual thinning and the success of the numerical solution in reproducing analytical solutions (Fig. 3) have motivated the decision to not include an analytical 0Moment0Shear boundary condition as part of gFlex v1.0.

The “0Slope0Shear” boundary condition (Fig. 4c) may be considered to be a flat clamp on the boundary of the plate that may be freely moved upwards or downwards. While it may require creative thought to uncover a geological process that holds a plate edge flat but allows it to move freely in the vertical, this boundary condition can also be used at an appropriate distance away from the load(s) to approximate a “NoOutsideLoads” boundary for a finite difference solution, though typically the 0Displacement0Slope boundary provides a closer match.

The “Periodic” boundary condition (Fig. 4d) wraps one side of the model around to the other side such that they form an infinite loop. Elastic thickness and loads both wrap around this boundary, making it possible to, if one is not careful, create sudden jumps in elastic thickness at the edge of the model. This takes somewhat longer to solve (Fig. 6c), but can be useful to compute a continuous mountain belt by modeling just a limited region perpendicular to the strike of the range crest; at the limit of a very narrow slice of model space, this approaches the 1-D line load solution. If a future model of lithospheric flexure relaxes the current assumption in gFlex that dx and dy may be different but must be constant in space, the Periodic boundary condition should enable global applications of flexural models. This is, in the best knowledge of the author, the first time that a Periodic boundary condition has been implemented for lithospheric flexure.

The “Mirror” boundary condition (Fig. 4e) reflects the elastic thickness and load structure across a plane of symmetry at the boundary. This may be used to speed a solution where a plane of mirror symmetry may be implied, which is important for large grids or where gFlex is used as part of a coupled set of numerical models (e.g., through CSDMS: Syvitski et al., 2011; Overeem et al., 2013; Peckham et al., 2013). Exam-

GMDD
8, 4245–4292, 2015

ple usage cases include topographic unloading by erosion of a symmetrical mountain range (Fig. 5c and d), isostatic adjustment under a symmetrical ice cap, and emplacement of a volcanic load. The latter two cases often have fully radial symmetry, and therefore may be placed at the corner of the solution array with Mirror boundary conditions on both adjacent sides to further limit the needed computational area. This is also to the best knowledge of the author the first application of a Mirror boundary condition to modeling of lithospheric flexure, which is surprising considering its potential utility.

The names of the boundary conditions are based on their effects on deflections, w, but solutions also require boundary conditions to be placed upon the flexural rigidity, D; these are listed in Table 1. For the 0Displacement0Slope, 0Slope0Shear, and 0Moment0Shear deflection boundary conditions, a 0-curvature flexural rigidity boundary condition has been chosen. This allows near-boundary gradients in flexural rigidity to be assumed to continue outside the computational domain. As noted above, Mirror and Periodic boundary conditions are applied to the rigidity field as well. For the analytical solutions, the approximation is an infinite plate of constant elastic thickness.

In two-dimensional solutions, boundary conditions meet at corners. Where a boundary condition meets another of the same boundary conditions at the corner, the two generate a continuous boundary condition that includes the corner of the array. This is always the case for the analytical solutions with implicit NoOutsideLoads boundary conditions. Where Mirror or Periodic boundary conditions meet themselves at corners, these produce doubly reflecting or doubly periodic boundaries; if every boundary is Mirror or Periodic (necessary in the latter case as Periodic boundary conditions must always exist as pairs on opposite sides), these generate an infinite tessellated plane of loads and elastic thicknesses. Some boundary conditions in gFlex can work harmoniously with others. Periodic and Mirror boundary conditions propagate 0Moment0Shear, 0Slope0Shear, and 0Displacement0Slope boundary conditions that exist orthogonally to them. Where Mirror and Periodic boundary conditions intersect at a corner, the Periodic boundary condition will propagate the Mirror boundary to $\pm\infty$. Those boundary conditions that do not reflect or repeat the effects of the other boundary

GMDD
8, 4245–4292, 2015

Flexure of the Lithosphere: gFlex v1.0

A. D. Wickert

conditions do not share the corners equally: In gFlex, 0Displacement0Slope boundary conditions dictate all corners where they meet other boundary conditions, forcing them to remain fixed at 0; physically, this means that the "clamp" of the 0Displacement0Slope boundary condition continues through the edges of the perpendicular boundaries. 0Moment0Shear boundary conditions were chosen control the corners where they meet 0Slope0Shear boundary conditions, as the 0Moment0Shear boundary condition has been recognized in geological work (e.g., Wessel, 1993; Burov et al., 1994; Stewart and Watts, 1997), while the 0Slope0Shear boundary condition has not.

2.4 Model benchmarking

A set of tests was performed to measure the speed at which gFlex computes solutions. In these tests, an elastic plate that is 1000 km long (1-D and 2-D) and 1000 km wide (2-D) is subjected to a square load at its center that ranges from 100 km to the full 1000 km on each side. This load places a normal stress of 9 702 000 Pa on the surface, which is equal to 300 m of mantle material (3300 kg m^{-3}). In these scenarios, there is no assumed infilling material ($\rho_f = 0$). gFlex computed solutions for uniform rectilinear grids of increasing size using gridded and ungridded superposition of analytical solutions (SAS and SAS_NG, respectively) and finite difference (FD) methods. All boundary conditions (Table 1 and Fig. 4) were tested, though not in combination. The finite difference solutions include scenarios with both constant (25 km) and variable (10–40 km) effective elastic thickness, with the latter varying sinusoidally over a wavelength of 500 km such that the plate contains two full T_e cycles. In the two-dimensional case, T_e varies in both dimensions to produce a smoothed checkerboard pattern of elastic thickness. Finite difference solutions reported employ the direct solver UMFPACK (Davis, 2004), as it is better-tested in gFlex than the iterative solution methods and is therefore the default solver. Figure 6 displays computation time for all of the benchmarking tests, and Fig. 7 is a comparison of the SAS_NG, SAS, and FD solution techniques for the case in which every point at which the solution is calculated also contains a nonzero load. These solution times do not account for file input or output or graphics generation. They do include the initialization time for the solution steps of gFlex, however, so a number of the power-law fits to solution time do not include the times calculated with the smallest arrays.

The factors that determine computation time are solution method and inclusion of Periodic boundary conditions. While the SAS_NG method scales the best with increasing grid size, it is so much slower than the other methods that it will not exceed their speed for any standard model runs. The finite difference method is the fastest if every cell contains a load, but can become slower than the analytical methods if only a few loads exist, as these latter methods must make one set of calculations across the grid per load. Standard runtimes are between a fraction of a second and a few minutes on a personal laptop computer (Dell XPS 13 Developer Edition running Ubuntu 14.10) (Figs. 6 and 7).

3 Model interfaces and coupling

Some users of gFlex may want to run a single calculation, while others may want to produce many solutions as part of a numerical model. Therefore, five different methods to use gFlex have been prepared:

1. standalone, with input files
2. as part of a Python script
3. driven by GRASS GIS (Neteler et al., 2012) to simplify integration of geospatially registered data with the lithospheric flexure model
4. as a component for the Community Surface Dynamics Modeling System (CSDMS) framework (Syvitski et al., 2011; Overeem et al., 2013; Peckham et al., 2013), including its tight integration into Landlab, a CSDMS-led Python-based Earth-surface modeling framework that is currently being developed (Hobley et al., 2013; Tucker et al., 2013).

GMDD
8, 4245–4292, 2015

GRASS GIS integration is also possible for model coupling using Python, including efforts that use the Landlab framework.

3.1 Standalone with input files

Some users may want to employ gFlex as a single calculation, for example to calculate the flexural response to a set of loads generated by a sedimentary deposit that was measured in the field. The user prepares an input file of model settings, an input ASCII grid of loads, and, should the elastic thickness be nonuniform, an input ASCII grid of lithospheric elastic thicknesses. Outputs from this mode of running gFlex include an ASCII grid of surface deflections and a set of plots of surface deflections and loads.

3.2 As part of a Python script

gFlex may also be imported as a Python module to be run either as a standalone simulation or as a component in a multi-model integration effort. This can be useful, for example, to use repeat forward modeling compute flexural solutions for sedimentary basin subsidence that best match the thicknesses of different sedimentary units. In this way, gFlex can be a flexural backstripping tool (see also Watts et al., 1982; Watts, 2001). This approach is also useful for scenarios in material infills a depression, but not over the whole domain and/or not with uniform density. This precludes the use of a constant ρ_f, and requires iteration to reach convergence. Examples of where this is useful include sedimentary basin deposition (see also Watts et al., 1982) and seawater loading at a shoreline (see also Mitrovica and Milne, 2003).

3.3 Driven by GRASS GIS

gFlex is also prepared for integration with the open-source geospatial software GRASS GIS (Neteler et al., 2012) as two "add-ons" or "extensions" named "r.flexure" and "v.flexure", which are raster and vector operations, respectively. As GRASS GIS is a map-based application, r.flexure and v.flexure employ two-dimensional solutions

GMDD
8, 4245–4292, 2015

(both analytical and finite difference), though future extension to flexure along chosen one-dimensional profiles would be possible. r.flexure can use the finite difference or SAS solution methods, whereas v.flexure exclusively uses the SAS_NG solution method to take advantage of its ability to produce solutions for an arbitrary scatter of loads points. Advantages of GRASS GIS include:

1. full integration within a geospatially registered environment, meaning that data can be directly used as model inputs, and that model outputs may be compared against data

2. a documented and standardized command-line interface

3. a pre-built and standardized graphical user interface (GUI).

The graphical user interface is incorporated into the GRASS GIS wxPython GUI (Landa, 2008; Neteler et al., 2012), and this is particularly helpful for researchers who are not as accustomed to command-line interaction with computers to use gFlex with their data. For computer modelers, the GRASS GIS coupling may be used within a broader framework of data–model integration (see, for example, Srinivasan and Arnold, 1994).

3.4 Modeling frameworks

CSDMS (broadly) and Landlab (in particular) both include methods for integrating modular blocks of code as part of their respective efforts towards the community-wide goal to make modeling of Earth systems less time-intensive and more streamlined (Voinov et al., 2010; Syvitski et al., 2011; Overeem et al., 2013; Peckham et al., 2013; Hobley et al., 2013; Tucker et al., 2013). gFlex is included as a modular component of the the still-in-development Landlab Earth-surface modeling framework (Hobley et al., 2013; Tucker et al., 2013). Landlab integration provides wrapping with the CSDMS Basic Model Interface (BMI) and Component Model Interface (CMI) using the CSDMS

Standard Name construction conventions (Peckham et al., 2013). The standard interfaces provided by both of these modeling frameworks will streamline model coupling that uses gFlex and help to prevent duplication of effort in building plate bending models. Furthermore, the inclusion of gFlex in Landlab will allow numerous Earth-surface systems to be modeled more precisely (Fig. 1).

4 Application example: Iceland

As a first example to utilize both the ability of gFlex to generate solutions with variable effective elastic thickness and its incorporation into GRASS GIS, gFlex is used along with a simple and efficient GIS-enabled glacier and ice cap model modified from the work of Colgan et al. (2015) to model a hypothetical expansion of the Iceland Ice Cap. While the importance of flexural isostasy in ice dynamics modeling has long been well-known (cf. Cuffey and Paterson, 2010), the author knows of no dynamic ice model that runs with a variable elastic thickness lithosphere, making this possibly the first such exercise. Earth's crust at Iceland has been built by the unique intersection of the Iceland hotspot and the Mid-Atlantic Ridge, and therefore presents cause to suspect the importance of heterogeneities in lithospheric strength that significantly impact solid Earth response to loading. Here I test the two-way coupling between ice dynamics and solid Earth deformation and the differences in steady-state ice caps that are produced in a modest climate change and ice cap extent scenario.

This coupled ice dynamics and flexural isostatic model of Iceland requires four input components: the elastic thickness structure around Iceland, the modern topography of Iceland, the modern surface temperature field of Iceland, and modern precipitation rates across Iceland. The ice cap model used here (cf. Colgan et al., 2015) employs a shallow-ice approximation with basal sliding as a linear function of driving stress, which is intentionally much simpler than the modeling approach that Hubbard et al. (2006) and Hubbard (2006) used to model the Last Glacial Maximum (LGM) Iceland ice cap. This is because the goal here is to show schematically the importance of

GMDD
8, 4245–4292, 2015

Flexure of the Lithosphere: gFlex v1.0

A. D. Wickert

including lateral variations in elastic thickness on the reconstructed thickness of an ice cap for a given paleoclimate, with less emphasis on actually reproducing any particular extent of the Iceland Ice Cap.

The elastic thickness structure under Iceland, in this schematic example, is related to the age of the oceanic crust following Calmant et al. (1990), who relates elastic thickness to age of the lithosphere by the simple equation:

$$T_e = (2.70 \pm 0.15)\sqrt{\Delta t} \tag{12}$$

where T_e is provided in km and the age of the lithosphere, Δt, is given in millions of years. As continental material also exists within the computational window, the elastic thickness map of Tesauro et al. (2012b, a) is used for all subaerial landmasses. Across the continental shelves, the oceanic-crust-based and Tesauro et al. (2012b, a) maps are blended using spline interpolation within GRASS GIS Neteler et al. (2012). The regional age of oceanic crust is provided by ridge in Iceland has an age of 6–7 Ma, resulting in a greater computed effective elastic thickness than would be expected based on the presence of the ridge or from heat flow data (e.g., Flóvenz and Saemundsson, 1993). While the structure of Iceland is certainly more complicated than the simpler parts of the ridge due to the effects of the hotspot and its tectonic environs (e.g., Watts and Zhong, 2000; Foulger, 2006), the assumption here is that the lithospheric effective elastic thickness structure due to the ridge is as if young crust continued along the Mid-Atlantic Ridge through all of Iceland, and the elastic thickness map (Fig. 8i) was modified to approximate this for the sake of this example.

The underlying digital elevation model, GEBCO_08 (British Oceanographic Data Centre , BaODC), includes the modern ice caps on Iceland, but these are already flexurally compensated and are small compared to the of the ice cap modeled here. While their removal would improve reconstructed ice discharge, they are ignored due to the schematic nature of this modeling effort.

Modern temperature and precipitation fields are from the Monthly NOAA-CIRES 20th Century Reanalysis (V2) by Compo et al. (2006, 2011) (for further background on their

GMDD
8, 4245–4292, 2015
Flexure of the Lithosphere: gFlex v1.0
A. D. Wickert

methods, see Whitaker and Hamill, 2002). These provide twentieth century mean conditions on a $2^{\circ} \times 2^{\circ}$-degree latitude/longitude grid (temperature) or a 94×192 Gaussian grid (precipitation). These were cast as point data and interpolated using splines in GRASS GIS (Neteler et al., 2012). Prior to this spline interpolation, temperature was projected to sea level using the mean cell elevation a lapse rate of $4.7\,^{\circ}\mathrm{C\,km^{-1}}$, following Anderson et al. (2014) for ice caps; after interpolation, the resultant temperatures were then interpolated up to their respective surface elevations using the same $4.7\,^{\circ}\mathrm{C\,km^{-1}}$ lapse rate. Although not all of the Icelandic surfaces are covered in ice at present, this rule was prescribed uniformly for the sake of a schematic model.

Three experiments were run: one with no flexure, one with flexure using a constant elastic thickness of 3.7 km (following Hubbard, 2006, and assuming $E = 65$ GPa), and one in which the full spatially variable flexure was used. In each of these runs, temperature was reduced from its present value by $5\,^{\circ}\mathrm{C}$ and ice expanded to cover an area approximately equal to the currently subaerially exposed continent, approximately consistent with the previous modeling results of Hubbard et al. (2006) and with a temperature change that is much less than the LGM drop of 10–13 °C that was predicted to cause ice to spread onto the continental shelves as well (Hubbard et al., 2006). Mass balance was simulated by a positive degree day melt model. June, July, and August temperatures were used to compute ablation, with a melt factor of $6\,\mathrm{mm\,d^{-1}\,K^{-1}}$. Precipitation was held constant and all precipitation was assumed to contribute to positive mass balance. Each scenario was run for 4000 years to reach full glacial and isostatic equilibrium, with isostatic equilibrium being assumed to occur instantaneously to facilitate more rapid computation of the equilibrium solution.

The results in Fig. 8 summarize the experiments. Figure 8c and f show the modeled flexural isostatic deformation and Fig. 8b and e show the deviation from the case with no isostasy; each of these pairs is for constant and variable elastic thickness, respectively. Figure 8h shows that with variable elastic thickness (Fig. 8i), ice thickness variability is concentrated where the elastic lithosphere has a low but finite thickness.

The example of isostatic response to ice advance in Iceland is just one possibility of a feedback between an Earth-surface (or other geological) process and flexural deformation. Further such scenarios involving, for example, orogenesis and foreland basin formation (in settings such as that studied by Ballato and Strecker, 2014), rifting (Braun et al., 2013), and river delta morphologic evolution (Kim et al., 2006), will improve our understanding of the dynamic interactions between Earth's surface and subsurface (e.g., Braun et al., 2013).

5 Model availability

gFlex is available from the University of Minnesota Earth-surface GitHub repository at https://github.com/umn-earth-surface/gFlex. It runs on Linux, Windows, and Mac computers running Python 2.(X≥7).Y. It may be downloaded as an archive that is a snapshot of the state of the code, or "cloned" into an updatable copy of the software on the computer of an end-user. Version 1.0, described in this paper, is stored at https://github.com/umn-earth-surface/gFlex/releases/tag/v1.0a (the alpha version release is for the Discussion Paper, and will be updated to a full release pending reviewer comments). gFlex is also stored on the Python Package Index (PyPI) at https://pypi.python.org/pypi/gFlex for easy automated download and installed with the command-line tool "pip". gFlex documentation is available in its file "README.md" that is displayed at the main GitHub repository page, and some additional information is presented at the gFlex CSDMS Wiki page at https://github.com/umn-earth-surface/gFlex.

Interfaces to GRASS GIS and Landlab are available from their respective repositories. The GRASS GIS interface works with GRASS GIS 7.X and can be downloaded and installed automatically with the "g.extension" tool within GRASS (Neteler et al., 2012) or be downloaded through the subversion repository at http://trac.osgeo.org/grass/browser/grass-addons/grass7. The Landlab interface is located in the Landlab GitHub repository at https://github.com/landlab/landlab/tree/master/landlab/components/gFlex.

6 Conclusions

gFlex is a new, open-source, easy-to-use model to compute isostatic deflections of Earth's lithosphere with uniform or nonuniform flexural rigidity due to arbitarily distributed surface loads. It can be run as a standalone model through a configuration file, a Python module, a component in the Landlab and CSDMS community modeling frameworks, or via one of two GRASS GIS add-ons for a direct link to geospatial data. Its open-source code base may be updated and improved by the community, it may be easily installed using automated tools, and it is poised to be coupled with other models in efforts to understand interactions between multiple components of the Earth system. These attributes all embody my primary aim in creating gFlex: to provide an accessible set of flexural isostatic solutions for work across the geosciences by field scientists and modelers alike.

Appendix A: Derivation

Plates and beams resist bending (i.e. flexure) through fiber stresses, which develop during loading-induced deformation. In this appendix, the background of the theory is provided by an abridged one-dimensional derivation, which provides the background to the assumptions made in both the analytical and finite difference one-dimensional and two-dimensional solutions. Components of the theoretical background will also be relevant to the various boundary condition options introduced in the main text.

A derivation of flexural response to a load can be subdivided into two components. The first is the bending moment, which describes the resistance of the plate to bending. The second is the relationship between the bending moment and the imposed load. For simplicity, these derivations will be presented for the one-dimensional case and then generalized to the two-dimensional case. This generalization is non-trivial only for the consideration of material properties in the bending moment derivation.

GMDD
8, 4245–4292, 2015

A1 Bending moments

The bending moment of a plate describes its resistance to being bent. This comes about because when a plate of finite thickness is bent, portions of the plate on the inside of the curve are placed under compression and portions of the plate on the outside of the curve are placed under tension. These fiber stresses ($\sigma_{x'x'}$ in the along-plate coordinate system x', z' depicted in Fig. A1) cause each infinitesimal layer of the plate to act like a spring that provides finite strength to the plate through which it resists bending.

Classical (Kirchhoff–Love) plate theory is derived using an approximation of cylindrical bending (cf. Love, 1888). Over short distances, the bent plate is assumed to follow the arc of a circle (Fig. A1). Arc length, s, is described as the product of the radius of curvature, r_c, and the angle over which the arc is defined, θ.

$$s = r_c\theta \tag{A1}$$

In a radial transect through a cylindrically bent plate of finite thickness, each level in the plate will have a different radius of curvature. At the midpoint of a single-layer plate (i.e. no changes in material properties with elevation z), such as that considered in this treatment of lithospheric flexure, the layer halfway between the top and the bottom of the plate will experience no net extension or shortening. This midpoint layer is therefore taken to be the reference radius of curvature, r_0, of a plate that extends from $r = -T_e/2$ to $r = T_e/2$, where T_e is the effective elastic thickness of the plate. To calculate the range of arc lengths, s, that exist above and below the reference layer at r_0, one can note that Eq. (A1) describes a linear relationship between arc length and radius of curvature. Therefore, it is possible to use the definition of strain and Eq. (A1) to define the "fiber strain" in each layer as a function of its distance from the midpoint. To do so, a Cartesian coordinate system (x', z') can be defined to exist along the curve of the bent plate (Fig. A1). The normal strain along the x' orientation, $\varepsilon_{x'x'}$, is given by:

$$\varepsilon_{x'x'} = \frac{s+\mathrm{d}s}{s} = \frac{(r-r_0)}{r_0} = \frac{z'}{r_0} \tag{A2}$$

Here, ds is the difference in arc length in a radial transect across the plate, r is an arbitrary radius, and θ has been dropped because it is constant and therefore cancels out. z' is defined to be zero at r_0. Sign conventions are unimportant due to the symmetry of the problem above and below the equilibrium layer (Fig. A1). To further express this system in terms of Cartesian coordinates that also allow for the cylindrical bending approximation to hold only locally, it becomes useful to reframe the cylindrical curvature expression in Eq. (A1) in terms of continuous Cartesian derivatives. To do so, the first step is to take the derivatives with respect to x of both sides of Eq. (A1) while allowing radius of curvature to be an imposed constant, and then approximate s as a linear segment to apply the distance formula. Note that here the coordinate system is (x,y), parallel and orthogonal, respectively, to the undeformed plate:

$$\frac{\mathrm{d}s}{\mathrm{d}x} = r\frac{\mathrm{d}\theta}{\mathrm{d}x} = \sqrt{1+\left(\frac{\mathrm{d}z}{\mathrm{d}x}\right)^2} \tag{A3}$$

One then uses the derivative of the trigonometric identity that $\theta = \arctan(\mathrm{d}z/\mathrm{d}x)$ to write:

$$\frac{\mathrm{d}\theta}{\mathrm{d}x} = \frac{\frac{\mathrm{d}^2z}{\mathrm{d}x^2}}{1+\left(\frac{\mathrm{d}z}{\mathrm{d}x}\right)^2} \tag{A4}$$

Noting that $(\mathrm{d}z/\mathrm{d}x) \ll 1$ for these long-wavelength and low-amplitude deflections of the lithosphere, this term vanishes from the derivation. It is then simple to combine and rearrange Eqs. (A3) and (A4) to show the intuitive result that smaller radii of curvature produce greater curvature. Further, by noting that derivatives of vertical position, z,

GMDD
8, 4245–4292, 2015

are identical to curvatures of deflection, w, from an initial position z_0, we can write the following equality:

$$\frac{1}{r} = \frac{d^2 z}{dx^2} = \frac{d^2 w}{dx^2} \tag{A5}$$

The next step is to connect these equations for bending into a framework of bending-related stresses and strains. In order to do so, it is first necessary to to show the approximate equality between terms depending on (x, y) and those depending on (x', y'). This is possible through the small angle approximation, which, combined with $(dz/dx) \ll 1$, means that:

$$\frac{dw}{dx} \approx \frac{dw}{dx'} \tag{A6}$$

and therefore, $dx \approx dx'$.

Equations (A2) and (A5) can be combined for $r = r_0$.

$$\varepsilon_{xx} = \varepsilon_{x'x'} = z' \frac{d^2 w}{dx^2} \tag{A7}$$

The equality between dx and dx' makes normal strains in both of these orientations be approximately equivalent, with ε_{xx} being the standard way of writing this strain for the remainder of this appendix. Equation (A7) becomes important in the final step to define the bending moment (first step next) in that it relates material strains directly to geometric positions that can be measured and/or modeled.

The bending moment itself, M, is the resistance of the plate to bending. It is defined as the sum through the thickness of the plate of all fiber stresses (x-oriented normal stresses) $\sigma_{x'x'}$ times their respective lever arms z' (cf. Turcotte and Schubert, 2002).

$$M = \int_{-T_e/2}^{T_e/2} \sigma_{xx} z' dz' \tag{A8}$$

GMDD
8, 4245–4292, 2015
Flexure of the Lithosphere: gFlex v1.0
A. D. Wickert

This definition of the bending moment of a plate shows that forces that initiate bending generate torques that oppose the bending. It is possible to rewrite this in terms of strain instead of stress by combining the one-dimensional elastic constitutive relationship (Hooke's Law) $\sigma_{xx} = E\varepsilon_{xx}$ with $1/(1-\nu^2)$. E is Young's modulus, which is a generalized spring constant that typically ranges between 10^{10} and 10^{11} for rock (Turcotte and Schubert, 2002, p. 106), and ν is Poisson's ratio, which describes how much material tends to extend (or shorten) in one direction when shortened (or extended) in another and is commonly taken to be 0.25 for the lithosphere (Turcotte and Schubert, 2002). The latter term involving Poisson's ratio is the result of the fact that for solutions on the Earth, the one-dimensional solution is assumed to apply for a plane (and loads) that continue indefinitely in the positive and negative y directions (i.e. into and out of the page in Fig. A1), but strain in this orientation is disallowed. Therefore, these compressive stresses that prevent y oriented bulging of the plate act to further inhibit its bending, effectively increasing the flexural rigidity.

$$M = \frac{E}{1-\nu^2}\int_{-T_\mathrm{e}/2}^{T_\mathrm{e}/2} \varepsilon_{xx} z' \mathrm{d}z' \tag{A9}$$

Both E and ν lie outside of the integral because they are assumed constant across z'.

It is possible to solve for the bending moment in one dimension by using Eq. (A7) to replace ε_{xx} in Eq. (A9). As the derivative $(\mathrm{d}^2z/\mathrm{d}x^2)$ is orthogonal to the direction of integration, the integral is simple to solve and results in a solution for the bending moment:

$$M = \frac{ET_\mathrm{e}^3}{12(1-\nu^2)}\frac{\mathrm{d}^2w}{\mathrm{d}x^2} \tag{A10}$$

The terms to the left of the derivative define the scalar flexural rigidity, D:

$$D = \frac{ET_\mathrm{e}^3}{12(1-\nu^2)} \tag{A11}$$

GMDD
8, 4245–4292, 2015

As D is very important in controlling flexural response and is a function of T_e, E, and ν, gFlex contains the additional simplifying assumption that E and ν are uniform constants. This permits variations in scalar flexural rigidity to map to variations in effective elastic thickness via Eq. (A11). It prevents overparameterization in gFlex, and implicitly states the assumption that changes in the effective elastic thickness of the lithosphere, cubed, are more significant than changes in Poisson's ratio, squared, or Young's modulus.

To generalize the bending moment to a two-dimensional plate, one must follow van Wees and Cloetingh (1994) in acknowledging that Poisson's ratio, ν, is applied differently to orientations parallel and perpendicular to those over which the bending occurs (normal moments) and is not important for the shear moments:

$$\mathbf{M}_\kappa = \begin{bmatrix} M_x \\ M_y \\ M_{xy} \end{bmatrix} = \mathbf{D} \begin{bmatrix} \frac{\partial^2 w}{\partial x^2} + \nu \frac{\partial^2 w}{\partial y^2} \\ \nu \frac{\partial^2 w}{\partial x^2} + \frac{\partial^2 w}{\partial y^2} \\ (1-\nu)\frac{\partial^2 w}{\partial x \partial y} \end{bmatrix} \tag{A12}$$

A2 Force and torque balance

A static lithospheric plate must balance the normal force, F, of imposed loads by generating shear forces, V and $V + \mathrm{d}V$, due to bending. In Fig. A1, the imposed load q is defined as:

$$q = \sum_{x}^{x+\mathrm{d}x} q(x) \tag{A13}$$

This signifies that in the numerical solution, a continuous load field is discretized into individual point loads of length dx and (if a 2-D solution is used) width dy. Further vertical normal stresses for plate flexure are generated by the the sum of the buoyant restoring force of displaced mantle, $\rho_m g w$, and additional driving forces by any surface

GMDD
8, 4245–4292, 2015

loads that fill the flexural depression, $\rho_f g w$. Here I explicitly ignore end loads because they are not part of the numerical solution in gFlex, which was designed with surface loads in mind, though they are straightforward to include (see van Wees and Cloetingh, 1994; Braun et al., 2013). Summed together, these form the additional term $\Delta\rho g w$, where $\Delta\rho = (\rho_m - \rho_f)$. The total shear force balance across a cell is therefore defined as:

$$\sum F = q + \Delta\rho g w + V - (V + \mathrm{d}V) = 0 \tag{A14}$$

$$\mathrm{d}V = q + \Delta\rho g w \tag{A15}$$

While the load stress, q, is directed downwards, its sign convention is flipped such that as observed geologic loads (e.g., sediments, volcanoes) increase in thickness, q increases as well.

These shear forces must be balanced in turn by the bending moments in a torque (τ) balance:

$$\sum \tau = -M + (M + \mathrm{d}M) + V \times 0 - (V + \mathrm{d}V) \times \mathrm{d}x = 0 \tag{A16}$$

$$V + \mathrm{d}V = \frac{\mathrm{d}M}{\mathrm{d}x} \quad (\mathrm{d}V \to 0) \tag{A17}$$

Equation (A17) states that the shear force (V: dV is vanishingly small in comparison) equals the derivative of the bending moment. The combination of Eqs. (A17) and (A10) shows that shear force is directly proportional to the third derivative of deflection:

$$V = \frac{\mathrm{d}M}{\mathrm{d}x} = D\frac{\mathrm{d}^3 w}{\mathrm{d}x^3} \tag{A18}$$

This observation is key to defining the 0Moment0Shear and 0Slope0Shear boundary conditions (Table 1 and Fig. 4).

After noting that $\mathrm{d}V \ll V$ and so can be neglected in Eq. (A17), Eqs. (A15) and (A17) can be combined by substituting V in Eq. (A15) to relate the bending moment to the

GMDD
8, 4245–4292, 2015

imposed loads q. When including the restoring force from mantle buoyancy, $\Delta\rho g w$, the resultant equation reads:

$$\frac{\mathrm{d}^2 M}{\mathrm{d}x^2} + \Delta\rho g w = q \tag{A19}$$

Equation (A19) can be combined with Eqs. (A10) and (A11) to show in the one-dimensional case that:

$$\frac{\mathrm{d}^2}{\mathrm{d}x^2}\left(D\frac{\mathrm{d}^2 w}{\mathrm{d}x^2}\right) + \Delta\rho g w = q \tag{A20}$$

In the more general two-dimensional case, one can create an analogous expression by separating the matrix flexural rigidity and curvatures used to create Eq. (A12) (van Wees and Cloetingh, 1994), resulting in:

$$\frac{1}{2}\left[\frac{\partial^2}{\partial x^2}\frac{\partial^2}{\partial y^2}\left(\frac{\partial^2}{\partial x \partial y} + \frac{\partial^2}{\partial y \partial x}\right)\right]\left(D\begin{bmatrix}1 & \nu & 0\\ \nu & 1 & 0\\ 0 & 0 & \frac{1-\nu}{2}\end{bmatrix}\begin{bmatrix}\frac{\partial^2 w}{\partial x^2}\\ \frac{\partial^2 w}{\partial y^2}\\ \frac{\partial^2 w}{\partial x \partial y} + \frac{\partial^2 w}{\partial y \partial x}\end{bmatrix}\right) + \Delta\rho g w = q \tag{A21}$$

Acknowledgements. A. D. Wickert greatly appreciates Eric Hutton's insights and help with CSDMS integration and project architecture as well as Daniel Hobley's work to integrate gFlex with Landlab. Václav Petráš' help in incorporating gFlex as an official set of GRASS GIS extensions was very much appreciated. Liam Colgan kindly supplied his glacier model source code, and conversations with Robert S. Anderson, Leif S. Anderson, and Gregory E. Tucker helped to inspire the project. 20th Century Reanalysis V2 data were provided by the NOAA/OAR/ESRL PSD, Boulder, Colorado, USA, from their Web site at http://www.esrl.noaa.gov/psd/. Funding for this project was provided by the US Department of Defense through the National Defense Science & Engineering Graduate Fellowship Program, the US National Science Foundation Graduate Research Fellowship under Grant No. DGE 1 144 083, an ExxonMobil geoscience grant, and by the Emmy Noether Programme of the Deutsche Forschungsgemeinschaft (DFG) through funds awarded to T. Schildgen under Grant No. SCHI 1241/1-1.

GMDD
8, 4245–4292, 2015
Flexure of the Lithosphere: gFlex v1.0
A. D. Wickert

References

Abramowitz, M. and Stegun, I.: Handbook of mathematical functions: with formulas, graphs, and mathematical tables, Courier Dover Publications, 1972. 4252

Airy, G. B.: On the computation the effect of the attraction of of mountain-masses disturbing apparent as the astronomical latitude of stations geodetic of surveys, Philo. Trans. Roy. Soc., 145, 101–104, 1855. 4247

Anderson, L. S., Roe, G. H., and Anderson, R. S.: The effects of interannual climate variability on the moraine record, Geology, 42, 55–58, doi:10.1130/G34791.1, 2014. 4264

Ballato, P. and Strecker, M. R.: Assessing tectonic and climatic causal mechanisms in foreland-basin stratal architecture: Insights from the Alborz Mountains, northern Iran, Earth Surf. Proc. Landf., 39, 110–125, doi:10.1002/esp.3480, 2014. 4265

Bernoulli, J. I. I.: Essai theorique sur les vibrations de plaques elastiques rectangularies et libres, Novi Commentari Acad Petropolit, 5, 197–219, 1789. 4247

Bodine, J. H. H., Steckler, M. S. S., and Watts, A. B. B.: Observations of flexure and the rheology of the oceanic lithosphere, J. Geophys. Res., 86, 3695–3707, doi:10.1029/JB086iB05p03695, 1981. 4248, 4249

Braun, C., Bezada, M., Braun, J., Deschamps, F., Rouby, D., and Dauteuil, O.: Flexure of the lithosphere and the geodynamical evolution of non-cylindrical rifted passive margins: Results from a numerical model incorporating variable elastic thickness, surface processes and 3D thermal subsidence, Tectonophysics, 604, 72–82, doi:10.1016/j.tecto.2012.09.033, 2013. 4248, 4249, 4265, 4272

British Oceanographic Data Centre (BaODC): The GEBCO_08 Grid, version 20100927, available at: http://www.gebco.net, 2010. 4263

Brotchie, J. F. and Silvester, R.: On crustal flexure, J. Geophys. Res., 74, 5240–5252, doi:10.1029/JB074i022p05240, 1969. 4252

Burov, E. B., Houdry, F., Diament, M., and Deverchere, J.: A broken plate beneath the north Baikal Rift Zone revealed by gravity modelling, Geophys. Res. Lett., 21, 129–132, doi:10.1029/93GL03078, 1994. 4255, 4258

Calmant, S., Francheteau, J., and Cazenave, A.: Elastic layer thickening with age of the oceanic lithosphere: a tool for prediction of the age of volcanoes or oceanic crust, Geophys. J. Int., 100, 59–67, doi:10.1111/j.1365-246X.1990.tb04567.x, 1990. 4263

Cauchy, A.-L.: Sur l'equilibre le mouvement d'une plaque solide, Exercises de Matematique, 3, 328–355, 1828. 4247
Colgan, W., Sommers, A., Rajaram, H., Abdalati, W., and Frahm, J.: Considering thermal-viscous collapse of the Greenland ice sheet, Earth's Future, doi:10.1002/2015EF000301, accepted, 2015. 4262
Comer, R. P.: Thick plate flexure, Geophys. J. Int., 72, 101–113, doi:10.1111/j.1365-246X.1983.tb02807.x, 1983. 4248
Compo, G. P., Whitaker, J. S., and Sardeshmukh, P. D.: Feasibility of a 100-year reanalysis using only surface pressure data, Bull. Am. Meteorol. Soc., 87, 175–190, doi:10.1175/BAMS-87-2-175, 2006. 4263
Compo, G. P., Whitaker, J. S., Sardeshmukh, P. D., Matsui, N., Allan, R. J., Yin, X., Gleason, B. E., Vose, R. S., Rutledge, G., Bessemoulin, P., BroNnimann, S., Brunet, M., Crouthamel, R. I., Grant, A. N., Groisman, P. Y., Jones, P. D., Kruk, M. C., Kruger, A. C., Marshall, G. J., Maugeri, M., Mok, H. Y., Nordli, O., Ross, T. F., Trigo, R. M., Wang, X. L., Woodruff, S. D., and Worley, S. J.: The Twentieth Century Reanalysis Project, Q. J. Roy. Meteorol. Soci., 137, 1–28, doi:10.1002/qj.776, 2011. 4263
Cuffey, K. M. and Paterson, W. S. B.: The physics of glaciers, Academic Press, Oxford, UK, 4th Edn., 2010. 4262
D'Acremont, E., Leroy, S., and Burov, E. B.: Numerical modelling of a mantle plume: The plume head-lithosphere interaction in the formation of an oceanic large igneous province, Earth Planet. Sci. Lett., 206, 379–396, doi:10.1016/S0012-821X(02)01058-0, 2003. 4247
Dalca, A. V., Ferrier, K. L., Mitrovica, J. X., Perron, J. T., Milne, G. A., Crevling, J. R., and Crevеling, J. R.: On Post-glacial Sea-Level - III: Incorporating Sediment Redistribution, Geophys. J. Int., 194, 45–60, doi:GJI-S-12-0692.R2, 2013. 4247
Davis, T. A.: Algorithm 832, ACM Transactions on Mathematical Software, 30, 196–199, doi:10.1145/992200.992206, 2004. 4249, 4250, 4254, 4258
Euler, L.: Tentamen de sono campanarum, Novi Commentarii Academiae scientiarum Imperialis Petropolitanae, 10, 261–281, 1764. 4247
Flóvenz, O. G. and Saemundsson, K.: Heat flow and geothermal processes in Iceland, Tectonophysics, 225, 123–138, doi:10.1016/0040-1951(93)90253-G, 1993. 4263
Flück, P.: Effective elastic thickness T_e of the lithosphere in western Canada, J. Geophys. Res., 108, 2430, doi:10.1029/2002JB002201, 2003. 4249

Fornberg, B.: Generation of finite difference formulas on arbitrarily spaced grids, Math. Comput., 51, 699–699, doi:10.1090/S0025-5718-1988-0935077-0, 1988. 4254

Foulger, G. R.: Older crust underlies Iceland, Geophys. J. Int., 165, 672–676, doi:10.1111/j.1365-246X.2006.02941.x, 2006. 4263

Germain, S.: Remarques sur la nature, les bornes et l'étendue de la question des surfaces élastiques et équation générale de ces surfaces, imprimerie de Huzard-Courcier, Paris, 1826. 4247

Gomez, N., Pollard, D., and Mitrovica, J. X.: A 3-D coupled ice sheet–sea level model applied to Antarctica through the last 40 ky, Earth Planet. Sci. Lett., 384, 88–99, doi:10.1016/j.epsl.2013.09.042, 2013. 4247

Göttl, F. and Rummel, R.: A Geodetic View on Isostatic Models, Pure Appl. Geophys., 166, 1247–1260, doi:10.1007/s00024-004-0489-x, 2009. 4247

Govers, R., Meijer, P., and Krijgsman, W.: Regional isostatic response to Messinian Salinity Crisis events, Tectonophysics, 463, 109–129, doi:10.1016/j.tecto.2008.09.026, 2009. 4247, 4248, 4251, 4254

Gunn, R.: A quantitative evaluation of the influence of the lithosphere on the anomalies of gravity, J. Franklin Institute, 236, 47–66, doi:10.1016/S0016-0032(43)91198-6, 1943. 4248

Heller, P. L., Angevine, C. L., Winslow, N. S., and Paola, C.: Two-phase stratigraphic model of foreland basin development, Geology, 16, 501–504, doi:10.1130/0091-7613(1988)016<0501:TPSMOF>2.3.CO;2, 1988. 4247

Hertz, H.: On the equilibrium of floating elastic plates, Ann. Phys. Chem., 22, 449–455, 1884. 4251

Hobley, D. E. J., Tucker, G. E., Adams, J. M., Gasparini, N. M., Hutton, E. W. H., Istanbulluoglu, E., and Siddhartha Nudurupati, S.: Landlab – a new, open-source, modular, Python-based tool for modeling landscape dynamics, Geological Society of America Abstracts with Programs, 45, p. 649, 2013. 4250, 4259, 4261

Hubbard, A.: The validation and sensitivity of a model of the Icelandic ice sheet, Quaternary Sci. Rev., 25, 2297–2313, doi:10.1016/j.quascirev.2006.04.005, 2006. 4262, 4264, 4291

Hubbard, A., Sugden, D., Dugmore, A., Norddahl, H., and Pétursson, H. G.: A modelling insight into the Icelandic Last Glacial Maximum ice sheet, Quaternary Sci. Rev., 25, 2283–2296, doi:10.1016/j.quascirev.2006.04.001, 2006. 4262, 4264

Jones, E., Oliphant, T., and Peterson, P.: SciPy: Open source scientific tools for Python, available at: http://www.scipy.org/, 2001. 4249, 4254

Karner, G. D. and Watts, A. B.: Gravity anomalies and flexure of the lithosphere at mountain ranges, J. Geophys. Res., 88, 10449, doi:10.1029/JB088iB12p10449, 1983. 4247

Kim, W., Paola, C., Voller, V. R., and Swenson, J. B.: Experimental measurement of the relative importance of controls on shoreline migration, J. Sediment. Res., 76, 270–283, doi:10.2110/jsr.2006.019, 2006. 4265

Kirby, J. and Swain, C.: Improving the spatial resolution of effective elastic thickness estimation with the fan wavelet transform, Comput. Geosci., 37, 1345–1354, doi:10.1016/j.cageo.2010.10.008, 2011. 4249

Kirby, J. F.: Estimation of the effective elastic thickness of the lithosphere using inverse spectral methods: The state of the art, Tectonophysics, 631, 87–116, doi:10.1016/j.tecto.2014.04.021, 2014. 4249, 4255

Kirby, J. F. and Swain, C. J.: A reassessment of spectral T_e estimation in continental interiors: The case of North America, J. Geophys. Res., 114, B08401, doi:10.1029/2009JB006356, 2009. 4249

Kirchhoff, G.: Ueber die Schwingungen einer kreisförmigen elastischen Scheibe, Ann. Phys., 157, 258–264, doi:10.1002/andp.18501571005, 1850. 4247, 4248

Lagrange, J. L.: Note communiquée aux Commissaires pour le prix de la surface élastique décembre 1811, Ann. Chimie Physique, 39, 149–151, 1828. 4247

Lambeck, K.: Flexure of the ocean lithosphere from island uplift, bathymetry and geoid height observations: the Society Islands, Geophys. J. Int., 67, 91–114, doi:10.1111/j.1365-246X.1981.tb02734.x, 1981. 4252

Landa, M.: New GUI for GRASS GIS based on wxPython, in: International Symposium GIS Ostrava, 2008. 4261

Le Meur, E. and Huybrechts, P.: A comparison of different ways of dealing with isostasy: examples from modeling the Antarctic ice sheet during the last glacial cycle, Ann. Glaciol., 23, 309–317, doi:10013/epic.12717.d001, 1996. 4247

Love, A. E. H.: The Small Free Vibrations and Deformation of a Thin Elastic Shell, Philos. Trans. Roy. Soc. A, 179, 491–546, doi:10.1098/rsta.1888.0016, 1888. 4248, 4267

Lowry, A. R. and Pérez-Gussinyé, M.: The role of crustal quartz in controlling Cordilleran deformation., Nature, 471, 353–357, doi:10.1038/nature09912, 2011. 4249

Luttrell, K. and Sandwell, D.: Ocean loading effects on stress at near shore plate boundary fault systems, J. Geophys. Res., 115, B08411, doi:10.1029/2009JB006541, 2010. 4247

May, G. M., Bills, B. G., and Hodge, D. S.: Far-field flexural response of Lake Bonneville from paleopluvial lake elevations, Phys. Earth Planet. Int., 68, 274–284, doi:10.1016/0031-9201(91)90046-K, 1991. 4247

McMillan, M. E., Angevine, C. L., and Heller, P. L.: Postdepositional tilt of the Miocene-Pliocene Ogallala Group on the western Great Plains: Evidence of late Cenozoic uplift of the Rocky Mountains, Geology, 30, 63–66, doi:10.1130/0091-7613(2002)030<0063:PTOTMP>2.0.CO;2, 2002. 4247

McNutt, M. K. and Menard, H. W.: Constraints on yield strength in the oceanic lithosphere derived from observations of flexure, Geophys. J. Int., 71, 363–394, doi:10.1111/j.1365-246X.1982.tb05994.x, 1982. 4252

Mitrovica, J. X. and Milne, G. A.: On post-glacial sea level: I. General theory, Geophys. J. Int., 154, 253–267, doi:10.1046/j.1365-246X.2003.01942.x, 2003. 4260

Müller, R. D., Sdrolias, M., Gaina, C., and Roest, W. R.: Age, spreading rates, and spreading asymmetry of the world's ocean crust, Geochem. Geophys. Geosyst., 9, 1–19, doi:10.1029/2007GC001743, 2008.

Neteler, M., Bowman, M. H., Landa, M., and Metz, M.: GRASS GIS: A multi-purpose open source GIS, Environ. Model. Softw., 31, 124–130, doi:10.1016/j.envsoft.2011.11.014, 2012. 4250, 4259, 4260, 4261, 4263, 4264, 4265

Oliphant, T. E.: Python for scientific computing, Comput. Sci. Eng., 9, 10–20, doi:10.1109/MCSE.2007.58, 2007. 4249

Overeem, I., Berlin, M. M., and Syvitski, J. P.: Strategies for integrated modeling: The community surface dynamics modeling system example, Environ. Model. Softw., 39, 314–321, doi:10.1016/j.envsoft.2012.01.012, 2013. 4250, 4256, 4259, 4261

Passey, Q. R.: Upper mantle viscosity derived from the difference in rebound of the Provo and Bonneville Shorelines: Lake Bonneville Basin, Utah, J. Geophys. Res., 86, 11701, doi:10.1029/JB086iB12p11701, 1981. 4247

Peckham, S. D., Hutton, E. W. H., and Norris, B.: A component-based approach to integrated modeling in the geosciences: The design of CSDMS, Comput. Geosci., 53, 3–12, doi:10.1016/j.cageo.2012.04.002, 2013. 4256, 4259, 4261, 4262

Pelletier, J. D.: Estimate of three-dimensional flexural-isostatic response to unloading: Rock uplift due to late Cenozoic glacial erosion in the western United States, Geology, 32, p. 161, 2004. 4248

Pérez-Gussinyé, M. and Watts, A. B.: The long-term strength of Europe and its implications for plate-forming processes, Nature, 436, 381–4, doi:10.1038/nature03854, 2005. 4249
Pérez-Gussinyé, M., Lowry, A. R., and Watts, A. B.: Effective elastic thickness of South America and its implications for intracontinental deformation, Geochem. Geophys. Geosyst., 8, Q5009, doi:10.1029/2006GC001511, 2007. 4249
Pérez-Gussinyé, M., Metois, M., Fernández, M., Vergés, J., Fullea, J., and a.R. Lowry: Effective elastic thickness of Africa and its relationship to other proxies for lithospheric structure and surface tectonics, Earth Planet. Sci. Lett., 287, 152–167, doi:10.1016/j.epsl.2009.08.004, 2009. 4249
Poisson, S.-D.: Mémoire sur l'équilibre et mouvement des corps élastiques, L'Académie des sciences, 1828. 4247
Pratt, J.: On the attraction of the Himalaya Mountains, and of the elevated regions beyond them, upon the plumb-line in India, Philos. Trans. Roy. Soc., 145, 53–100, 1855. 4247
Royden, L. and Karner, G. D.: Flexure of Lithosphere Beneath Apennine and Carpathian Foredeep Basins: Evidence for an Insufficient Topographic Load, AAPG Bulletin, 68, 704–712, doi:10.1306/AD461372-16F7-11D7-8645000102C1865D, 1984. 4248, 4249
Sacek, V. and Ussami, N.: Reappraisal of the effective elastic thickness for the sub-Andes using 3-D finite element flexural modelling, gravity and geological constraints, Geophys. J. Int., 179, 778–786, doi:10.1111/j.1365-246X.2009.04334.x, 2009. 4248
Srinivasan, R. and Arnold, J. G.: Integration fo a basin-scale water quality model with GIS, J. Am. Water Res. Assoc., 30, 453–462, doi:10.1111/j.1752-1688.1994.tb03304.x, 1994. 4261
Stephenson, R.: Flexural models of continental lithosphere based on the long-term erosional decay of topography, Geophys. J. Int., 77, 385–413, doi:10.1111/j.1365-246X.1984.tb01940.x, 1984. 4251
Stephenson, R. and Lambeck, K.: Isostatic response of the lithosphere with in-plane stress: Application to central Australia, J. Geophys. Res., 90, 8581–8588, doi:10.1029/JB090iB10p08581, 1985. 4251
Stewart, J. and Watts, A. B.: Gravity anomalies and spatial variations of flexural rigidity at mountain ranges, J. Geophys. Res., 102, 5327–5352, 1997. 4247, 4248, 4255, 4258
Syvitski, J., Hutton, E., Peckham, S., and Slingerland, R.: CSDMS – A modeling system to aid sedimentary research, The Sedimentary Record, 9, 4–9, doi:10.2110/sedred.2011.1.4, 2011. 4250, 4256, 4259, 4261

Tassara, A., Swain, C., Hackney, R., and Kirby, J.: Elastic thickness structure of South America estimated using wavelets and satellite-derived gravity data, Earth Planet. Sci. Lett., 253, 17–36, doi:10.1016/j.epsl.2006.10.008, 2007. 4249

Tesauro, M., Kaban, M. K., and Cloetingh, S. A. P. L.: How rigid is Europe's lithosphere?, Geophys. Res. Lett., 36, L16303, doi:10.1029/2009GL039229, 2009. 4249

Tesauro, M., Audet, P., Kaban, M. K., Brgmann, R., and Cloetingh, S.: The effective elastic thickness of the continental lithosphere: Comparison between rheological and inverse approaches, Geochem. Geophys. Geosyst., 13, 1–18, doi:10.1029/2012GC004162, 2012a. 4249, 4263

Tesauro, M., Kaban, M. K., and Cloetingh, S. A. P. L.: Global strength and elastic thickness of the lithosphere, Glob. Planet. Change, 90-91, 51–57, doi:10.1016/j.gloplacha.2011.12.003, 2012b. 4249, 4263

Tesauro, M., Kaban, M. K., and Cloetingh, S. a. P. L.: Global model for the lithospheric strength and effective elastic thickness, Tectonophysics, 602, 78–86, doi:10.1016/j.tecto.2013.01.006, 2013. 4249, 4255

Timoshenko, S., Woinowsky-Krieger, S., and Woinowsky, S.: Theory of plates and shells, McGraw–Hill, New York, 2nd Edn., 1959. 4248, 4250

Todhunter, I. and Pearson, K.: A History of the Theory of Elasticity and of the Strength of Materials, from Galilei to the Present Time, vol. 35, Cambridge University Press, Cambridge, England, UK, doi:10.1038/035313a0, 1886. 4247

Tucker, G. E., Hobley, D. E., Gasparini, N. M., Hutton, E., Istanbulluoglu, E., Nudurupati, S., and Adams, J. M.: Creative Computing with Landlab: Open-Source Python Software for Building and Exploring 2D Models of Earth-Surface Dynamics, in: AGU Fall Meeting Abstracts, p. D2, 2013. 4250, 4259, 4261

Turcotte, D. L. and Schubert, G.: Geodynamics, Cambridge University Press, 2nd Edn., 2002. 4250, 4269, 4270

Van der Lee, S.: High-resolution estimates of lithospheric thickness from Missouri to Massachusetts, USA, Earth Planet. Sci. Lett., 203, 15–23, doi:10.1016/S0012-821X(02)00846-4, 2002. 4248

van der Walt, S., Colbert, S. C., and Varoquaux, G.: The NumPy Array: A Structure for Efficient Numerical Computation, Comput. Sci. Eng., 13, 22–30, doi:10.1109/MCSE.2011.37, 2011. 4249

GMDD
8, 4245–4292, 2015

van Rossum, G. and Fred L. Drake, J.: The Python Language Reference Manual, Python Software Foundation, version 2nd Edn., 2012. 4249
van Wees, J. D. and Cloetingh, S.: A Finite-Difference Technique to Incorporate Spatial Variations In Rigidity and Planar Faults Into 3-D Models For Lithospheric Flexure, Geophys. J. Int., 117, 179–195, doi:10.1111/j.1365-246X.1994.tb03311.x, 1994. 4248, 4249, 4250, 4253, 4271, 4272, 4273
Vening Meinesz, F. A.: Une nouvelle methode pour la reduction isostatique regionale de l'intensite de la pesanteur, Bulletin Géodésique (1922–1941), 29, 33–51, 1931. 4248, 4251
Vening Meinesz, F. A.: Gravity Over the Hawaiian Archipelago and Over the Madeira Area, in: Proceedings of the Koninklijke Nederlandse Akademie van Wetenschappen, vol. 44, 1–14, 1941. 4248
Vening Meinesz, F. A.: Les graben africains, résultat de compression ou de tension dans la croûte terrestre, Bull. Inst. R. Colon. Belge, 21, 539–552, 1950. 4248
Ventsel, E., Krauthammer, T., and Carrera, E.: Thin Plates and Shells: Theory, Analysis, and Applications, vol. 55, Marcel Drecker, Inc., doi:10.1115/1.1483356, 2002. 4247
Voinov, A. A., DeLuca, C., Hood, R. R., Peckham, S., Sherwood, C. R., and Syvitski, J. P. M.: A Community Approach to Earth Systems Modeling, Eos, Transactions American Geophysical Union, 91, 117–118, doi:10.1029/2010EO130001, 2010. 4261
Watters, T. R. and McGovern, P. J.: Lithospheric flexure and the evolution of the dichotomy boundary on Mars, Geophys. Res. Lett., 33, L08S05, doi:10.1029/2005GL024325, 2006. 4246
Watts, A. B.: An analysis of isostasy in the world's oceans 1. Hawaiian-Emperor Seamount Chain, J. Geophys. Res., 83, 5989, doi:10.1029/JB083iB12p05989, 1978. 4246
Watts, A. B.: Isostasy and Flexure of the Lithosphere, Cambridge Univ Press, 2001. 4246, 4247, 4248, 4260
Watts, A. B. and Zhong, S.: Observations of flexure and the rheology of oceanic lithosphere, Geophys. J. Int., 142, 855–875, doi:10.1046/j.1365-246x.2000.00189.x, 2000. 4246, 4248, 4263
Watts, A. B., Karner, G. D., and Steckler, M. S.: Lithospheric Flexure and the Evolution of Sedimentary Basins, Philos. Trans. Roy. Soc. A, 305, 249–281, doi:10.1098/rsta.1982.0036, 1982. 4247, 4260

GMDD
8, 4245–4292, 2015

Flexure of the Lithosphere: gFlex v1.0

A. D. Wickert

Welch, P.: The use of fast Fourier transform for the estimation of power spectra: A method based on time averaging over short, modified periodograms, IEEE Transactions on Audio and Electroacoustics, 15, 70–73, doi:10.1109/TAU.1967.1161901, 1967. 4251

Wernicke, B. and Axen, G. J.: On the role of isostasy in the evolution of normal fault systems, Geology, 16, 848, doi:10.1130/0091-7613(1988)016<0848:OTROII>2.3.CO;2, 1988. 4247

Wessel, P. I.: A reexamination of the flexural deformation beneath the Hawaiian Islands, J. Geophys. Res., 98, 12 177, doi:10.1029/93JB00523, 1993. 4255, 4258

Whitaker, J. S. and Hamill, T. M.: Ensemble Data Assimilation without Perturbed Observations, Mon Weather Rev., 130, 1913–1924, doi:10.1175/1520-0493(2002)130<1913:EDAWPO>2.0.CO;2, 2002. 4264

Wickert, A. D.: Flexure version 0.6, doi:10.1594/IEDA/100123, available at: http://csdms.colorado.edu/wiki/Model:Flexure, 2012. 4248, 4249

GMDD

8, 4245–4292, 2015

Flexure of the Lithosphere: gFlex v1.0

A. D. Wickert

Table 1. Boundary conditions. Names provided here are the same as those used in the model. The first five can be selected for numerical solutions. The final one, NoOutsideLoads, is the outcome of superposition of analytical solutions, which allows the entire space to respond to local loads as if the 0-deflection boundaries were infinitely far away. In this notation, the subscript b indicates the boundary, generically. Where 0 and n are included as subscripts, i.e. for the Mirror and Periodic boundary conditions, these indicate boundaries at the first and last node of the model domain along a particular axis. Subscript x, which is a stand-in for x or y, is a variable distance to indicate the symmetry across a Mirror boundary. Each of these boundary conditions requires a corresponding boundary condition for flexural rigidity.

Name	Mathematical	Description	Rigidity b.c.
0Displacement0Slope	$w_\mathrm{b} = 0$	No displacement at boundaries	$\frac{\mathrm{d}^2 D_\mathrm{b}}{\mathrm{d}x^2} = 0$
0Moment0Shear	$\frac{\mathrm{d}^2 w_\mathrm{b}}{\mathrm{d}x^2} = \frac{\mathrm{d}^3 w_\mathrm{b}}{\mathrm{d}x^3} = 0$	Broken plate with a free cantilever end	$\frac{\mathrm{d}^2 D_\mathrm{b}}{\mathrm{d}x^2} = 0$
0Slope0Shear	$\frac{\mathrm{d}w_\mathrm{b}}{\mathrm{d}x} = \frac{\mathrm{d}^3 w_\mathrm{b}}{\mathrm{d}x^3} = 0$	Free displacement of a horizontally clamped boundary	$\frac{\mathrm{d}^2 D_\mathrm{b}}{\mathrm{d}x^2} = 0$
Mirror	$w_{\mathrm{b}=n-x} = w_{\mathrm{b}=n+x}$	Plane of mirror symmetry at boundary	$D_{\mathrm{b}=n-x} = D_{\mathrm{b}=n+x}$
Periodic	$w_{\mathrm{b}=n} = w_{\mathrm{b}=0}$	Wrap-around boundary: infinite tiling of model domain	$D_{\mathrm{b}=n} = D_{\mathrm{b}=0}$
NoOutsideLoads	$w_\infty = 0$	Produced by analytical solutions with uniform D	$\frac{\mathrm{d}D_\mathrm{b}}{\mathrm{d}x} = 0$

GMDD
8, 4245–4292, 2015

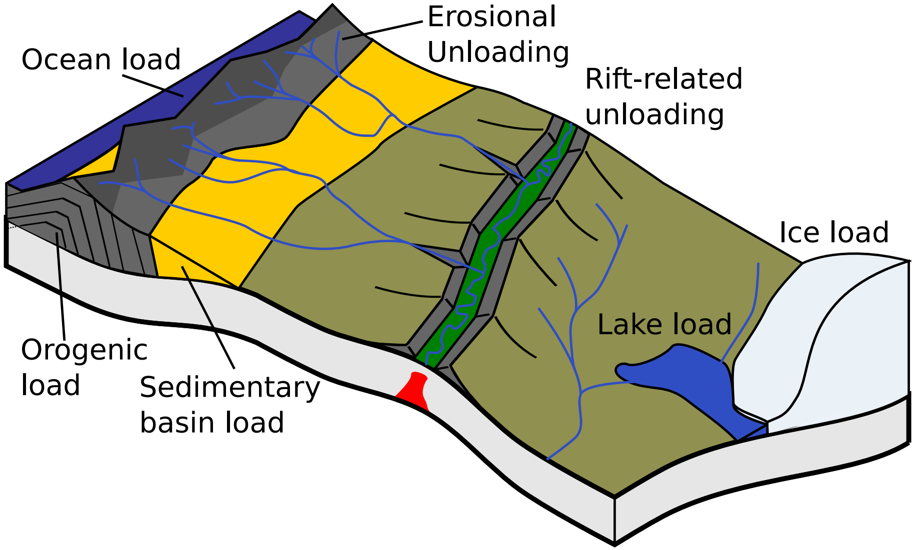

Figure 1. Flexural isostasy can be produced in response to a range of geological loads.

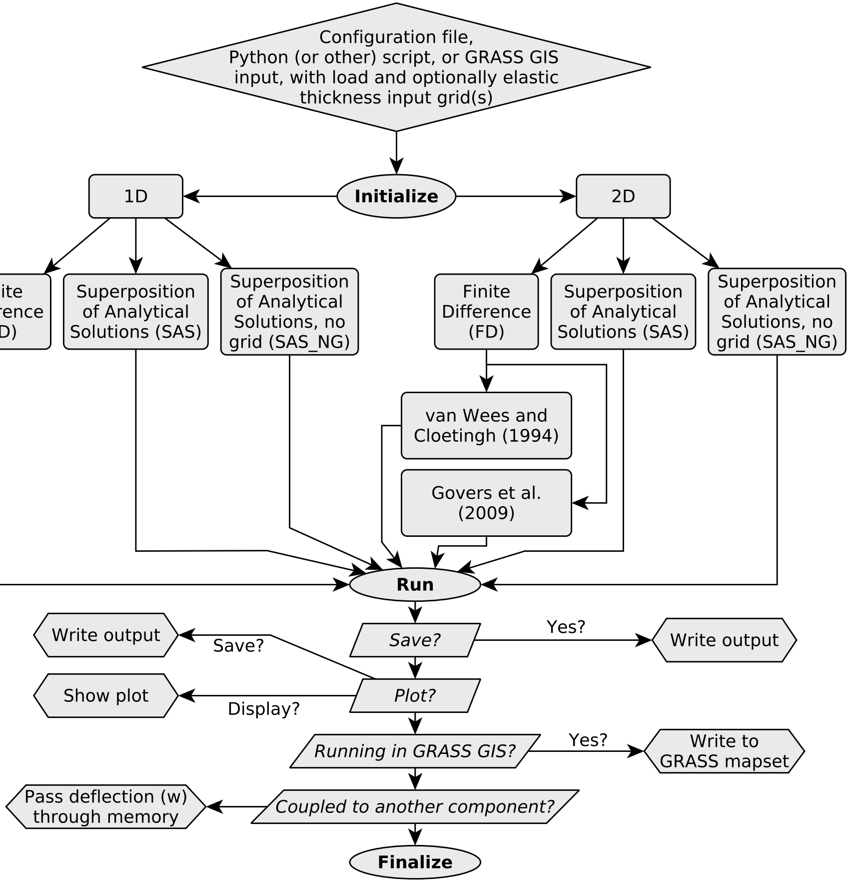

Figure 2. Flowchart for gFlex as (1) a standalone model with configuration and input files, (2) a Python module or coupled component in a modeling framework, or (3) a GRASS GIS component.

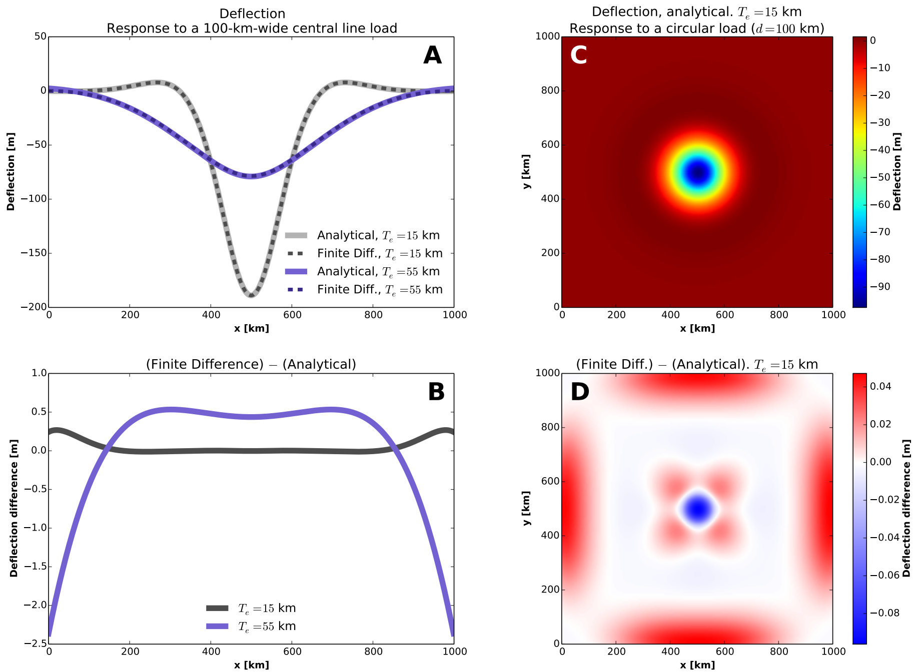

Figure 3. Numerical (FD) and analytical (SAS) solutions in 1-D **(a)** and 2-D **(c)** and their differences (**b** and **d**) in response to a 100 km-(long/in-diameter) central line/circular load. These differences are due primarily to the NoOutsideLoads boundary condition of the analytical solution and the 0Displacement0Slope boundary condition of the numerical solution. This can be seen in **(b)** where the example with a lower elastic thickness is less-offset due to the greater number of flexural wavelengths between the load and the boundary, and in the greater agreement between the solutions on the longer diagonal boundaries in **(d)**. The offset in the middle, visible as a small bump in **(b)** and a blue diamond surrounded by red petals in **(d)**, is due to the difference between approximating the load as a sum of point impulses (analytical) and as the solution to a rectangularly gridded matrix equation based on the same theory (numerical).

GMDD
8, 4245–4292, 2015

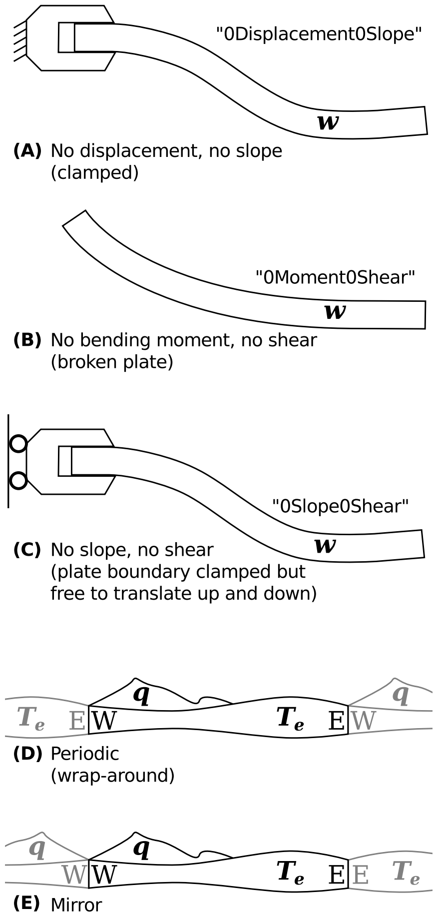

Figure 4. Schematics of boundary condition types allowed in the finite difference solutions to gFlex.

GMDD
8, 4245–4292, 2015

Flexure of the Lithosphere: gFlex v1.0

A. D. Wickert

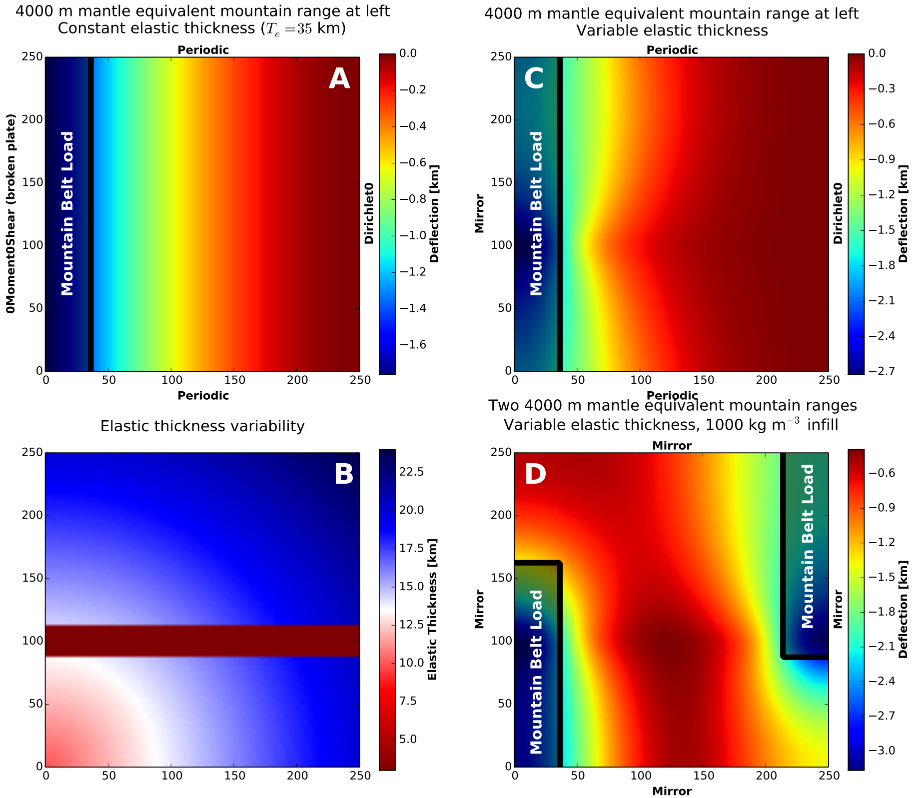

Figure 5. Example runs of gFlex with varying elastic thickness and boundary conditions. **(a)** depicts a long north–south mountain belt and foreland basin under uniform elastic thickness. **(b)** provides a contrived field of variable elastic thickness. **(c)** is similar to **(a)** except in that it uses a Mirror boundary for a symmetrical mountain belt over a continuous lithospheric plate instead of a broken plate solution and that the plate has variable elastic thickness. **(d)** depicts the flexural interaction of two mountain belts on the same variable elastic thickness lithosphere by employing Mirror boundary conditions at all edges.

GMDD
8, 4245–4292, 2015

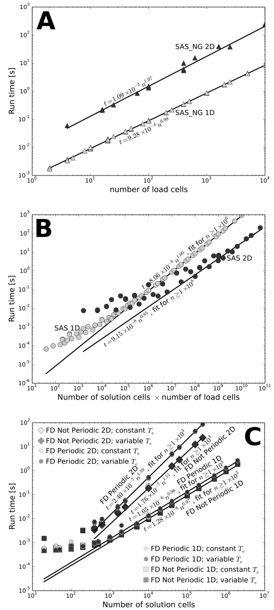

Figure 6. Model benchmarking. The ungridded superposition of analytical solutions (SAS_NG) computation time is proportional to the number of cells with loads are present ("load cells"), as the solutions are calculated once for each of these positions. The gridded superposition of analytical solutions (SAS) scales to the total number of grid cells ("solution cells") times the number of load cells, as this is the total number of computations that must be made. Finite difference solutions are computed with sparse matrices with dimensions equal proportional to the grid dimensions, squared, and therefore scale with the number of total grid cells. All of the solution time relationships are close to linear except for the two-dimensional finite difference solutions, due to the added complexity of their finite difference stencil. Many fits are to a subset of the data to avoid those solutions that are so rapid that the amount of time required for the non-solver portions of the code becomes significant. All marker symbols are semi-transparent, meaning that darker symbols than those that appear in the legend imply additional data points underneath.

GMDD
8, 4245–4292, 2015
Flexure of the Lithosphere: gFlex v1.0
A. D. Wickert

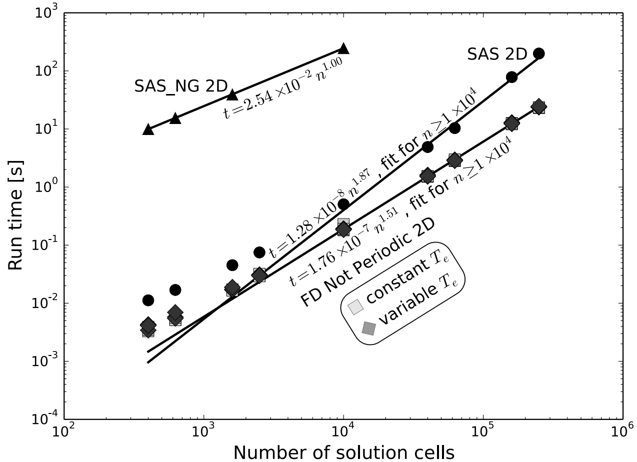

Figure 7. Comparison between solution methods where every cell in the domain contains a load. The ungridded superposition of analytical solutions (SAS_NG) scales best but in these tests is the slowest. It can, however, be faster when fewer cells contain loads. Some fits are to a subset of the data to avoid those solutions that are so rapid that the amount of time required for the non-solver portions of the code becomes significant. All marker symbols are semi-transparent, meaning that darker symbols than those that appear in the legend imply additional data points underneath.

GMDD

8, 4245–4292, 2015

Flexure of the Lithosphere: gFlex v1.0

A. D. Wickert

Title Page
Abstract | Introduction
Conclusions | References
Tables | Figures
◀| |▶
◀ ▶
Back | Close
Full Screen / Esc
Printer-friendly Version
Interactive Discussion

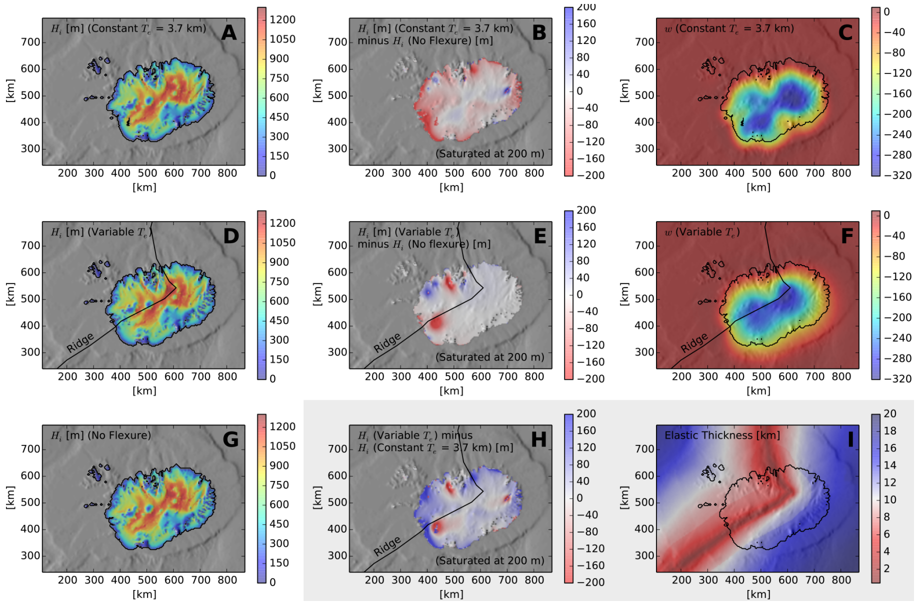

Figure 8. This coupled model run for a hypothetical extent of the Iceland ice cap shows the influence of a variable elastic thickness structure **(i)**. The areal extent of the three ice caps is nearly identical **(a, d, g)** in this small-scale and largely topographically controlled example. Flexural isostasy with a constant 3.7 km elastic thickness **(c)** (following Hubbard, 2006) reduces ice cap extent and causes some interior ice thickening when compared to the case without flexure **(b)** as the ice cap conforms to the bowl-shaped depression that it creates. Deformation in the case with variable elastic thickness **(f)** focuses along the ridge and extends farther on the southwestern side that has greater elastic thickness, and modifies the topography of western Iceland (low elastic thickness) to produce spatially variable ice thickness changes **(e, h)**.

GMDD
8, 4245–4292, 2015

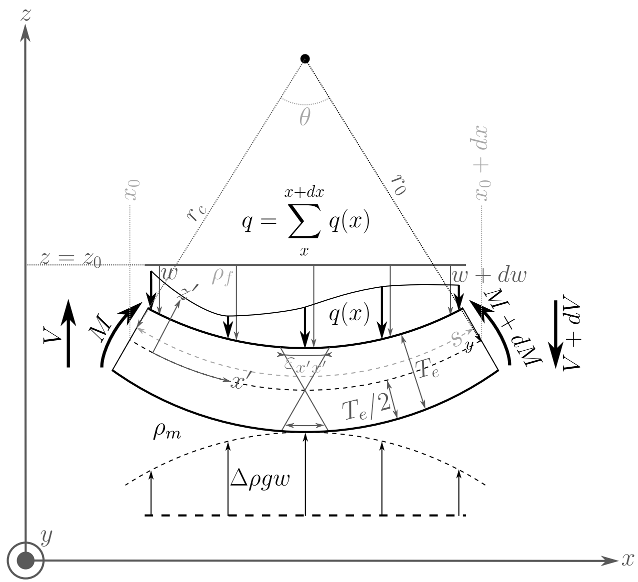

Figure A1. Schematic of the bending of a buoyant plate under a load that is long in the y-orientation.

Discussion Paper | Discussion Paper | Discussion Paper | Discussion Paper |

GMDD

8, 4245–4292, 2015

Flexure of the Lithosphere: gFlex v1.0

A. D. Wickert